Supplementary Information:
Morphology and Composition of Cholesterol-rich Micellar Nanostructures Determine Transmembrane Protein (GPCR) Activity

Michelle A. O'Malley, Matthew E. Helgeson, Norman J. Wagner, Anne S. Robinson

Protein Production and Purification. The human adenosine A_2a receptor (hA_2aR) was heterologously expressed in yeast with a C-terminal decahistidine tag to facilitate purification via immobilized metal affinity chromatography. $hA_2aR\text{-}His_{10}$ was purified to greater than 98% from yeast membranes as judged by Coomassie staining following mechanical lysis and surfactant solubilization as described previously[1].

Mixed Micelle Preparation. All materials were purchased from Anatrace, at the highest purity available. Unless otherwise noted, stock solutions were prepared in 50 mM sodium phosphate buffer, pH 7.0. A 10 wt % aqueous stock solutions was prepared for DDM. Stock solutions of cholesteryl hemisuccinate (CHS) were made in 3-(3-cholamidopropyl)-dimethylammoniopropane sulfonate (CHAPS) to create a solution that was 6% CHAPS/1.2% CHS (wt%). For small angle neutron scattering experiments, stock solutions were prepared in 50 mM sodium phosphate buffer, pH 7.0 in D_2O in order to enhance contrast.

In order to test different ratios of CHAPS/CHS in micelles, the parameter δ was defined, as given by:

$$\delta = \frac{\text{mass of CHAPS} + \text{mass of CHS}}{\text{mass of surfactant} + \text{mass of CHAPS} + \text{mass of CHS}}. \quad \text{(S1)}.$$

All solutions were prepared at a fixed total concentration of 1 wt% solute by massing the appropriate amounts of the stock solutions and diluting with buffer in H_2O or D_2O, as needed. Samples were prepared with both DDM/CHAPS/CHS and DDM/CHAPS without CHS at equivalent values of δ in order to isolate the effects of CHS addition as distinct from the effects of CHAPS addition.

Surfactant Exchange for $hA_2aR\text{-}His_{10}$. $hA_2aR\text{-}His_{10}$ was solubilized from the yeast membrane environment using 2% dodecyl-beta-D-maltoside (DDM) (Anatrace, Maumee, OH) containing 1% CHAPS (Anatrace) and 0.2% cholesteryl hemisuccinate tris salt (CHS) (Anatrace). After solubilization, His-tagged hA_2aR was bound to nickel resin (Qiagen, Valencia, CA), and surfactant concentrations were reduced to 0.1% DDM, 0.1% CHAPS, and 0.02% CHS as done previously during low-concentration imidazole washes[1]. Following the last 50 mM imidazole wash, equal amounts of resin-bound protein were aliquoted, and different surfactant systems (at various concentrations) were introduced. Surfactant exchange was accomplished by settling nickel resin via centrifugation for 1-2 minutes at 3,000 g, removing the supernatant surfactant mixture by careful pipetting with gel-loading tips, and resuspending the nickel resin in fresh surfactant (or surfactant mixture). To ensure that sufficient surfactant exchange was achieved, samples were washed 4-5 times in this fashion where each wash was generally greater than 100x resin volumes.

Activity Measurements for $hA_2aR\text{-}His_{10}$. Competitive ligand binding was employed to evaluate activity of purified adenosine $hA_2a\text{-}His_{10}$ receptors stabilized in different surfactant systems while immobilized on nickel resin. Samples were divided into equal volumes, with an ultimate dilution of approximately 2 – 4 μL settled resin per mL of surfactant solution prior to the assay. 180 μL of resin-bound protein samples were loaded onto 96-well Multi-screen filter B plates (Millipore, Billerica, MA), and were combined with 20 μL ligand mixture. To generate a full competitive binding curve, this mixture consisted of 25 nM ^{3}[H]-CGS-21,680 (Perkin Elmer, Waltham, MA) and increasing concentrations of N^6-cyclohexyladenosine (CHA) (Sigma, St. Louis, MO), as done previously for

hA_2aR competitive binding experiments[1]. Point competition measurements were also made, where resin-bound hA_2aR-His_{10} samples were incubated with 25 nM ^{3}[H]-CGS-21,680 alone and with 25 nM ^{3}[H]-CGS-21680 in the presence of 1 mM CHA (~ 2000 x K_d). The K_d for CGS-21,680 association with hA_2aR is approximately 49 nM [1]. The specific binding for these samples was calculated by subtracting radioactive counts obtained in the presence of competitor from counts obtained from binding to radio-ligand alone. Ligand incubation was allowed to proceed for 1.5-2 hours at room temperature with gentle agitation on a rotating orbital mixer. Following incubation, samples were filtered, and washed at least 3 times with 200 µL of the appropriate surfactant buffer. Radioactive counts were determined by scintillation counting on a Perkin Elmer MicroBeta Jet. Samples were run in triplicate, and the error was calculated as the standard deviation among these replicates. Non-specific binding was determined by measuring binding to the same amount of resin in 0.1% DDM, 0.1% CHAPS, and 0.02% CHS, in the absence of bound protein.

Raw competitive radio-ligand binding data is shown in Figure S1 for purified hA_2aR solubilized in DDM ($\delta = 0$), DDM/CHAPS ($\delta = 0.55$), and DDM/CHAPS/CHS micelles ($\delta = 0.55$). Note that ligand binding activity is only observed for DDM/CHAPS/CHS.

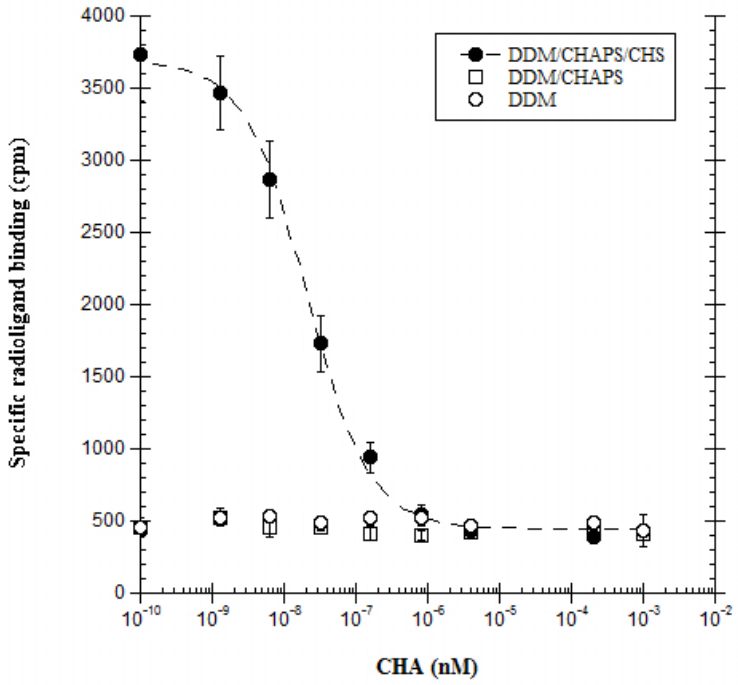

Figure S1: Competitive radio-ligand binding assay comparing relative activity of purified hA_2aR in DDM (open circles), DDM/CHAPS (open squares), and DDM/CHAPS/CHS (closed circles) micelles.

Small Angle Neutron Scattering (SANS). SANS experiments were performed at the Center for Neutron Science at the National Institute of Standards and Technology (NIST) in Gaithersburg, MD. Mixed micelle samples were loaded into 2 mm quartz window titanium scattering cells. Measurements were made on the NG3 and NG7 30m SANS instruments, using a temperature-controlled sample block (CB10) held at 25 ºC. The incident neutron beam had a mean wavelength of $\lambda = 6$ Å, with a resolution of $\Delta\lambda/\lambda = 0.11$. The scattered intensity of samples was collected on a 2-dimensional detector at three different detector distances: 1.35 m, 4.5 m, and 13.1 m. Data were reduced according to standard protocols using the NCNR Igor software package[2], resulting in absolute scattered intensities, *I(q)*, where q is the scattering vector $q = 4\pi \sin(\theta/2)/\lambda$ and θ is the scattering angle.

Figure S2 shows the measured scattering spectra for each of the values of δ studied for both DDM/CHAPS/CHS micelles (top) and DDM/CHAPS (micelles). Model independent fitting of the low-q data (Figure 1, inset) using a Guinier analysis[3],

$$\ln\left[I(q)-I_b\right]=\ln I(0)-\frac{q^2R_g^2}{3} \qquad \text{(S2)}$$

to determine the radius of gyration, R_g, of the micelles as well as the zero-angle intensity, *I(0)*, where the incoherent background intensity, I_b, was determined by Porod analysis of the high-q portion of the scattering spectra[4, 5] (not shown). The best-fit values of *I(0)* and R_g are listed in Table S1 for DDM/CHAPS/CHS micelles and in Table S2 for DDM/CHAPS micelles in the absence of CHS. Both quantities exhibit a monotonic decrease with increasing δ, consistent with an overall decrease in size of the micellar aggregates upon addition of CHAPS/CHS. Note that this decrease is more pronounced for DDM/CHAPS in the absence of CHS, suggesting that CHS tends to counteract the effects of CHAPS on micelle morphology.

In order to obtain the micellar shape and aggregation numbers, a shape-dependent model was used to analyze the scattering spectra. We assume monodisperse scattering objects of uniform composition and isotropic orientation, such that the total scattered intensity of neutrons from the micellar solution is given by:

$$I(q)=\phi_p P(q)S(q)+I_b, \qquad \text{(S3)}$$

where ϕ_p is the volume fraction of scattering objects, *P(q)* is the form factor, and *S(q)* is the structure factor. We further assume that the micelles are sufficiently dilute that interparticle interactions can be neglected, such that *S(q)* = 1. n_p and P(q) are determined by fitting scattering data to models for specific micelle morphologies. I_b is essentially a background scattering measurement, and is typically determined from a Porod plot.

The scattering spectra were best-fit by an oblate ellipsoidal model for *P(q)*, given by

$$P(q)=\frac{1}{V_p}\left(\Delta\rho_n\right)^2\int_0^1 f^2\left[qb\left(1+x^2\left(\frac{a^2}{b^2}-1\right)\right)^{1/2}\right]dx \qquad \text{(S4)}$$
$$f(x)=3V_p\frac{\sin x-x\cos x}{x^3}$$

where *a* and *b* are the major and minor axes of the ellipsoid, respectively, $V_p=4\pi a^2 b/3$ is the volume of the ellipsoid, and $\Delta\rho_n = \rho_{n,tot} - \rho_{n,D2O}$ is the neutron contrast factor given by the difference in scattering length density of the micelle, $\rho_{n,tot}$, and the solvent, $\rho_{n,D2O}$. The model given by eq. (S4) was fit using non-linear least squares regression to obtain the model parameters *a*, *b*, and $\Delta\rho_n$ (Table S1). For fitting, it was assumed that the volume fraction of micelles is fixed by

$$\phi_p=\sum_i\frac{w_i\rho_s}{\rho_i}, \qquad \text{(S5)}$$

where w_i and ρ_i are, respectively, the mass fraction and density of component *i* in solution, ρ_s is the solvent (buffer) density, and the sum is over all species in the solvent. The values of ρ_i, as well as other properties of materials used for further calculations are listed in Table S3. The resulting best-fit values

of a, b, and $\Delta\rho$ are listed in Table S1 for DDM/CHAPS/CHS micelles and in Table S2 for DDM/CHAPS micelles in the absence of CHS. Statistical errors in the calculation of SANS fit parameters are also indicated. Note that the radius of gyration for the oblate ellipsoidal micelles, $R_g^2 = \left(2a^2 + b^2\right)/5$, calculated from the model fit is in quantitative agreement with that determined by Guinier analysis for all conditions (Table S1), thereby validating the chosen morphology of the micelles.

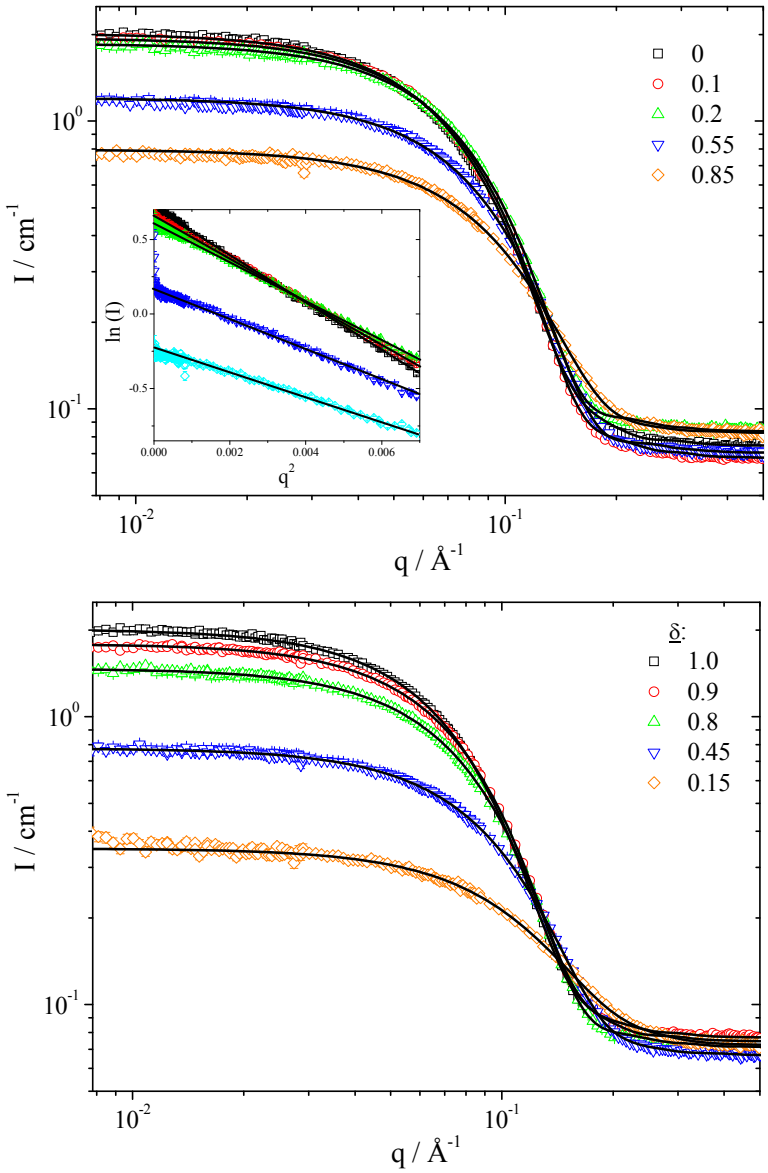

Figure S2. SANS spectra for DDM/CHAPS/CHS micelles (top) and DDM/CHAPS micelles (bottom) for the values of δ indicated. Points represent measured intensities and lines represent fits to the uniform oblate ellipsoid model described in the text. Inset: Scaled plots of ln(I) versus q^2 used for Guinier analysis.

Table S1. Structural parameters of DDM/CHAPS/CHS micelles determined by SANS

δ	$I(0)$ [cm^{-1}]	a [Å]	b [Å]	R_g [1] [Å]	R_g [2] [Å]	V_p [10^3Å^3]	$\Delta\rho_n$ [10^{-7} cm^{-2}]	N_{DDM}	N_{CHAPS}	N_{CHS}
0	2.035	32.37±0.04	17.54±0.05	21.9±0.4	22.3±0.2	77.0±0.3	7.43	121±1	-	-
0.1	1.922	30.56±0.06	18.31±0.05	20.9±0.5	20.3±0.2	71.7±0.3	7.37	96±1	7±1	3±1
0.2	1.853	29.53±0.05	18.59±0.06	20.3±0.4	19.8±0.3	67.1±0.3	7.26	82±1	12±1	5±1
0.55	1.193	26.45±0.05	17.15±0.07	18.4±0.4	17.4±0.2	50.3±0.3	6.84	34±1	27±1	12±1
0.85	0.791	24.76±0.06	13.87±0.08	16.8±0.4	15.4±0.1	35.6±0.3	6.44	10±1	29±1	9±1

[1] Determined by oblate ellipsoid model fit.
[2] Determined by Guinier analysis.

Table S2. Structural parameters of DDM/CHAPS micelles determined by SANS

δ	$I(0)$ [cm^{-1}]	a [Å]	b [Å]	R_g [1] [Å]	R_g [2] [Å]	V_p [10^3Å^3]	$\Delta\rho_n$ [10^{-7} cm^{-2}]	N_{DDM}	N_{CHAPS}	N_{CHS}
0	2.035	32.37±0.04	17.54±0.05	21.9±0.4	22.3±0.2	77.0±0.3	7.43	121±1	-	-
0.1	1.786	30.19±0.03	17.70±0.04	20.7±0.3	20.1±0.2	67.5±0.3	7.38	93±1	4±1	-
0.2	1.457	28.54±0.04	17.58±0.05	19.7±0.3	19.0±0.2	59.9±0.3	7.29	74±1	11±1	-
0.55	0.776	24.47±0.06	13.84±0.06	16.7±0.6	16.0±0.2	34.7±0.3	6.92	25±1	21±1	-
0.85	0.347	21.51±0.06	8.80±0.08	14.2±0.8	12.5±0.1	17.0±0.4	6.54	4±1	17±1	-

[1] Determined by oblate ellipsoid model fit.
[2] Determined by Guinier analysis.

In order to determine the aggregation number, N_i, for each component in the micelles, it was assumed that (1) each component is distributed uniformly within the micelle interior and (2) the micelle is completely dehydrated (no D_2O is present in the micelle interior). Accordingly, since the quantities $I(0)$, V_p, and $\Delta\rho$ represent independent measures of the micelle scattering, shape, and composition, respectively, we define a system of three linearly independent equations,

$$\begin{aligned} I(0) &= \phi_p \left(\sum_i N_i v_i \right) \left(\sum_i \left(\rho_{n,i} - \rho_{n,D2O} \right) \right)^2 \\ V_p &= \sum_i N_i v_i \\ \left(\Delta\rho \right)^2 &= \left(\sum_i \left(\rho_{n,i} - \rho_{n,D2O} \right) \right)^2 \end{aligned} \qquad \text{(S6)}$$

where v_i and $\rho_{n,i}$ are, respectively, the molecular volume and scattering length density of species i, and the sums are over all components in the micelle (DDM, CHAPS, and CHS). The first balance is that on the absolute zero-angle intensity, the second balance is that on the volume of a single micelle, and the third balance is that on the scattering length density of a single micelle. These microscopic balance equations were solved given the known values of $I(0)$, V_p, and $\Delta\rho$ using a custom Matlab routine. Since the non-linear set of equations given by (S6) has multiple solutions, only those that satisfied $\{N_i\} > 0$ and $N_{CHAPS} > N_{CHS}$ were assumed to be valid. Note that this approach yields results that are significantly different than would be obtained by assuming ideal mixing of each species within the micelles due to the large disparity in CMC between DDM, CHAPS, and CHS.

Table S3. Properties of molecular components used in SANS data analysis

Compound	Chemical Formula	Molar mass [g/mol]	ρ [kg/m^3]	ρ_n [10^{-7} cm^{-2}]	v [Å^3]
D_2O	D_2O	20.03	1017	63.0	-
DDM	$C_{24}H_{46}O_{11}$	510.6	1227	7.43	691.0
CHAPS	$C_{31}H_{58}N_2O_7S$	614.9	937	6.33	830.3
CHS	$C_{31}H_{50}O_4$	486.7	1060	5.76	501.8

We note several important aspects of the measured micelle morphology. First, the aggregation number of DDM for $\delta=0$ is in agreement with that previously reported for pure DDM micelles [6]. Similarly, the aggregation number of CHAPS in the DDM/CHAPS micelles approaches that measured previously for pure CHAPS micelles in the limit of $\delta \rightarrow 1$ [7]. These findings give strong validation of the method used to calculate the aggregation numbers of the various components. We also note that the addition of CHAPS and CHAPS/CHS generally gives rise to a decrease in the aspect ratio of the oblate ellipsoidal micelles. Once again, this effect is less pronounced in the presence of CHS. These results show that whereas CHAPS tends to increase spontaneous curvature of the micelles, CHS tends to preserve lower curvature, suggesting that the hydrophobic moieties of CHS are oriented parallel to the minor access of the ellipsoidal aggregate.

References.

1. O'Malley, M. A.; Lazarova, T.; Britton, Z. T.; Robinson, A. S., High-level expression in Saccharomyces cerevisiae enables isolation and spectroscopic characterization of functional human adenosine A(2)a receptor. *Journal of Structural Biology* **2007,** 159, (2), 166-178.
2. Kline, S. R., Reduction and analysis of SANS and USANS data using IGOR Pro. *Journal of Applied Crystallography* **2006,** 39, 895-900.
3. Guinier, A.; Fournet, G., *Small angle scattering of X-rays*. 1st Ed. ed.; Wiley: New York, 1955.
4. Kratky, O.; Porod, G., Rontgenuntersuchung Geloster Fadenmolekule. *Recueil Des Travaux Chimiques Des Pays-Bas-Journal of the Royal Netherlands Chemical Society* **1949,** 68, (12), 1106-1122.
5. Porod, G., Die Rontgenkleinwinkelstreuung Von Dichtgepackten Kolloiden Systemen .1. *Kolloid-Zeitschrift and Zeitschrift Fur Polymere* **1951,** 124, (2), 83-114.
6. Timmins, P. A.; Leonhard, M.; Weltzien, H. U.; Wacker, T.; Welte, W., A Physical Characterization of Some Detergents of Potential Use for Membrane-Protein Crystallization. *Febs Letters* **1988,** 238, (2), 361-368.
7. le Maire, M.; Champeil, P.; Moller, J. V., Interaction of membrane proteins and lipids with solubilizing detergents. *Biochimica Et Biophysica Acta-Biomembranes* **2000,** 1508, (1-2), 86-111.